Multiferroic memory effect far above the Néel temperature in single-crystal $Gd_{0.5}Dy_{0.5}MnO_3$

Chandan De,[1] Rabindranath Bag,[2] Surjeet Singh,[2] and A. Sundaresan[1,*]
[1]*School of Advanced Materials and Chemistry and Physics of Materials Unit, Jawaharlal Nehru Centre for Advanced Scientific Research, Jakkur P.O., Bangalore 560064, India*
[2]*Indian Institute of Science Education and Research, Pashan, Pune 411008, India*

(Received 15 April 2019; revised manuscript received 22 July 2019; published 4 September 2019)

The memory effect of the polarized ferroelectric domain state in a nonpolar spin-density wave phase has been reported in few multiferroics and the origin of this effect has been attributed to the presence of polar nanodomains in the nonpolar magnetic state. From magnetoelectric and dielectric-relaxation studies, we show the presence of the memory effect beyond the antiferromagnetic ordering temperature ($T_N^{Mn} = 39.5$ K) in a single crystal of $Gd_{0.5}Dy_{0.5}MnO_3$. We suggest that the Debye-like relaxation behavior, which is a manifestation of localized charge carries or polar nanodomains in the crystal, is responsible for the memory effect. Intriguingly, a correlation of dielectric relaxation behavior to the magnetic interactions is found in a wide range of temperature including noncollinear spin-induced ferroelectric, the collinear nonpolar antiferromagnetic, as well as in the paramagnetic states.

DOI: 10.1103/PhysRevB.100.104407

I. INTRODUCTION

Multiferroic materials are currently a major area of research in condensed-matter physics where both the ferroelectric and magnetic polarizations coexist with a strong coupling between them [1–6]. Besides, great attention has been paid to these materials due to their potential for applications in memory devices, spintronics, sensors, and magnetoelectric microwave devices as well as for fundamental physics [7–11]. Recently, in cycloidal magnetic ordering induced multiferroic materials such as $MnWO_4$, $YMnO_3$-thin film, and rare-earth (R) manganites, a novel memory effect was observed where the materials can store their polarization domain states in a disordered nonferroelectric state [12–14]. Specifically, when the material is polarized macroscopically by external electric field, the polarized single-domain state should remain only in the ferroelectric region, as the ferroelectric dipoles would be randomly oriented above T_C. Remarkably, it was first observed in $MnWO_4$ by Taniguchi *et al.* that the ferroelectric polarization state could be retrieved from the paraelectric collinear antiferromagnetic state by magnetic-field cycling. It was proposed that there could be a small ferroelectric embryo, which has a microscopically polarized chiral domain state preserved even in the paraelectric collinear antiferromagnetic state due to a high degree of magnetic frustration in the material [12]. Later, Fina *et al.* reported a similar memory effect in the collinear antiferromagnetic region in another chiral ordered multiferroic $Sm_{0.5}Y_{0.5}MnO_3$ and argued with the same hypothesis. The consideration of such noncollinear domains or chiral component in the collinear phase in R-manganite multiferroics is befitting as the polar transition between noncollinear to collinear state is suggested to be an order-disorder type [15]. This was supported through various studies, for example, a fluctuating ferroelectric region in the sinusoidal phase as anticipated through a model calculation showing a dynamic short-range order (cycloidal type) in the collinear sinusoidal range ($T_C < T < T_N$) [16]. Terahertz spectroscopic studies also evidenced a nonzero dielectric contribution of electromagnons in the sinusoidal phase [11,17]. It was found from soft x-ray-scattering study that the transition of incommensurate and commensurate state (T_C or $T_{lock-in}$) in $TbMnO_3$ is between two noncollinear states of Mn^{3+} ions, suggesting the presence of microscopic noncollinear state in a collinear matrix [18]. Thus, the observation of memory effect was explained quite satisfactorily through the small embryo model. Further, through neutron-diffraction study of electric-field poled chiral domain state in the ferroelectric state of $MnWO_4$, it was found that the domains can remember their chirality even in the paramagnetic state [19]. Later, the memory effect was observed up to a deep paramagnetic state in another mixed rare-earth manganite [20]. All these studies indirectly support the presence of polar chiral embryo in the nonferroelectric state. Therefore, it is important to further explore the origin of this memory effect.

Here, we unambiguously confirm the presence of the memory effect above T_N, i.e., in the paraelectric as well as paramagnetic region in a single crystal of $Gd_{0.5}Dy_{0.5}MnO_3$ (GDMO) multiferroic. This material exhibits unique magnetoelectric properties where it shows polarization along $a-$ and c directions due to the tilted cycloidal plane [21]. We demonstrate that a typical relaxation behavior that corresponds to localized charge carriers or polar nanodomains is responsible for the memory effect. We have shown how an internal electric field created due to such charge carriers can polarize the ferroelectric dipoles even in the paramagnetic phase. Finally, a model consisting of different types of dipoles in the material is provided in order to explain the memory effect over the entire temperature range of interest.

*sundaresan@jncasr.ac.in

II. EXPERIMENTAL

Single crystal was grown by floating-zone technique as described in our earlier work [21]. Here we used polished platelike samples of [100] or [001] orientations with dimension of about 2 mm × 2 mm × 0.3 mm. All the electrical measurements were performed in a Quantum Design Physical Property Measurement System. Dielectric permittivity and pyrocurrent properties were studied by Agilent E4980A Precision LCR meter and Keithley electrometer/high-resistance meter (6517A), respectively. Electrical contacts were made using silver paste (PELCO high-performance silver paste).

III. RESULTS AND DISCUSSION

A. Observation of memory effect

Heat capacity divided by temperature (C/T) versus temperature (T) data shown in Fig. 1 (left axis) ensured the three successive magnetic transitions at $T_N^{Mn} = 39.5$ K, $T_{Cy}^{Mn} = 16$ K (T_C), and $T_N^{RE} = 5$ K, corresponding to sinusoidal antiferromagnetic, noncollinear cycloidal ordering (ferroelectric onset, T_C), and short-range ordering of rare-earth moments, respectively, at zero magnetic field as reported recently [21]. The spontaneous polarization, occurring predominantly along a axis at the transition from collinear sinusoidal to spiral ordering of Mn^{3+} spins, is shown in the right axis of Fig. 1 where P_a decreases below the short-range ordering of rare-earth moments. In order to demonstrate the memory effect, we first present the pyrocurrent behavior along the a axis (Fig. 2). The measurement protocol for this study is as follows: First, the sample was poled with an electric field (E_{ext}) from 30 to 7 K to avoid the intricacy that may arise due to the effect of magnetic ordering of the R ions on the polarization. Next, the electric field was removed from the sample and the electrodes were kept shorted at 7 K for 30 min to remove the stray charges on the sample-electrode interface. Finally, the electrometer was connected to the sample and the current was recorded through continuously ramping the temperature from 7 K to various temperatures ($T_R = 25$, 35, 45, 55, 65, 75, 80, and 90 K) (Fig. 2) and cooling back to 7 K without further application of external electric or magnetic fields. Remarkably, depolarization current peaks with negative sign

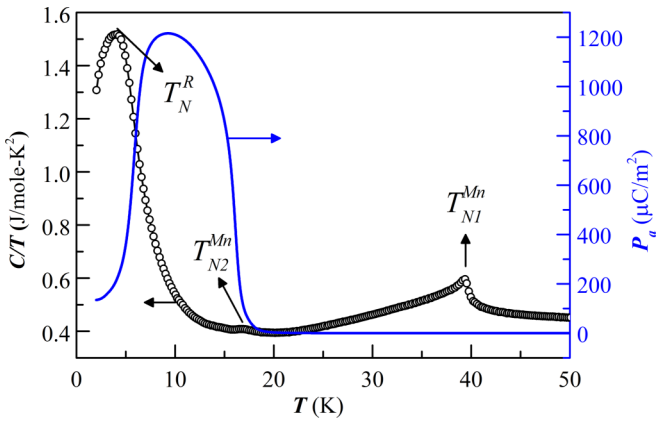

FIG. 1. Heat capacity divided by temperature (left axis) and electric polarization (right axis) as a function of temperature.

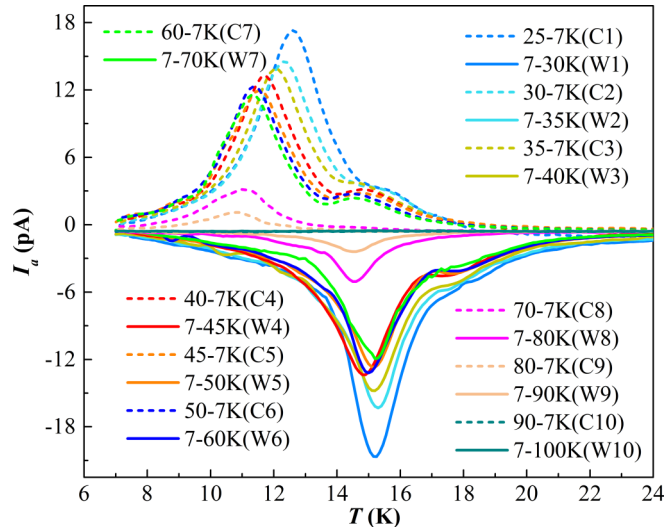

FIG. 2. Pyrocurrent behavior while warming (continuous curve) and cooling (dotted curve) from 7 K to various temperatures (T_R) after initial poling the sample from 30 to 7 K with −5 kV/cm, 0 T.

occur while warming (continuous curve, denoted as W_n, the so-called pyrocurrent peak) and polarization current peaks with positive sign occur while cooling (dotted curve, denoted as C_n) at the onset of ferroelectric ($T_C \sim 16$ K) for T_R as high as 80 K which is twice the antiferromagnetic ordering temperature of Mn^{3+} spins. For $T_R = 80$ K, no trace of these peaks was found in both the cooling and warming cycles. Since the sample was poled with electric field only in the first cooling from 30 to 7 K and the pyrocurrent peak persists in the subsequent warming and cooling cycles even after warming the sample up to 80 K, the memory of the polarization state is restored from far above the Curie temperature ($T_C \sim 16$ K) and thus this behavior can be called the memory effect.

To examine quantitatively the thermal remnant of polarization (denoted as P^{TR}) with different ramping temperature (T_R) we performed a slightly modified experiment. In this case, the sample was poled for every single measurement in the beginning while cooling from 30 to 7 K and the pyrocurrent was recorded while warming the sample. Thus, the first and second steps were the same as before. In the third step, the temperature was ramped to T_R and cooled to 7 K without applying any external electric or magnetic field. Finally, the electrometer was connected to the sample and the current was recorded while warming the sample from 7 to 30 K. This procedure was followed for all the T_R to obtain the pyrocurrent feature for all the individual ramping temperatures. We obtained the P^{TR} after integrating the pyrocurrent (inset of Fig. 3) for all the T_R [Figs. 3(a) and 3(b)]. In order to visualize the temperature dependence of the polarization, the polarization obtained at 8 K is shown as a function of T_R in Fig. 3(c). We notice that the P^{TR} decreases initially with increasing T_R up to ∼35 K. With further increase of temperature, it shows a steplike increase and remains nearly invariant up to 60 K and gradually vanishes at 80 K. It is remarkable that both the experiments exhibit the signature of polarization memory up to the ramping temperature 80 K, demonstrating the salient memory effect. We also confirmed

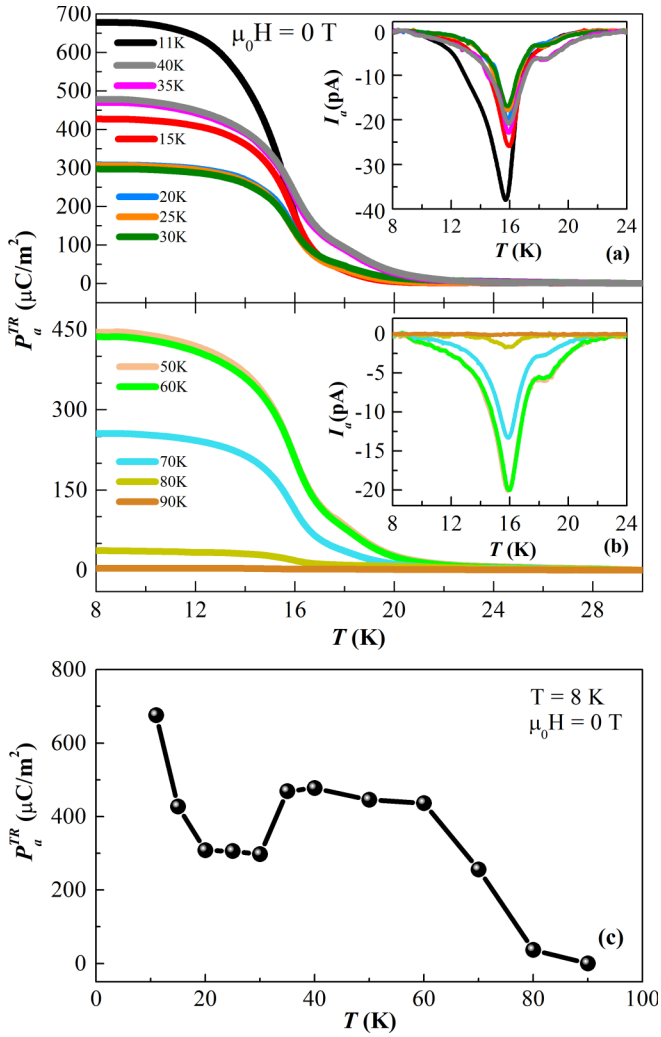

FIG. 3. Polarization vs temperature data along [100] direction after poling the sample from 30 to 8 K with 5.6 kV/cm and 0 T magnetic field and shorting the electrode at 8 K for 30 min and ramping the temperature from 8 K to different T_R to 8 K. (a) For $T_R < T_N$ and (b) for $T_R > T_N$. Insets shows the corresponding recorded pyrocurrent data. (c) Thermal remnant polarization (P_a^{TR}) value at 8 K as a function of temperature.

the memory effect along the c axis since this material shows polarization along both $a-$ and c axes (see Supplemental Material, Fig. S1 [22]).

B. Dielectric relaxation

In order to investigate the origin of the memory effect above T_N, we looked at the dielectric response with frequency along $a-$ and c directions. The frequency-dependent dielectric constant along the a axis shows the typical-peak related to ferroelectricity at the cycloidal ordering temperature ($T_C = 16$ K) [Figs. 4(a) and 4(b)]. Above T_C, it exhibits almost temperature-independent behavior up to 100 K. Intriguingly, along the c axis, in addition to the anomaly associated with the ferroelectricity, the dielectric data show a frequency-dependent steplike increase in the real part (ε'). This behavior of ε' (in Fig. 4, the real part is labeled as ε and not ε') is

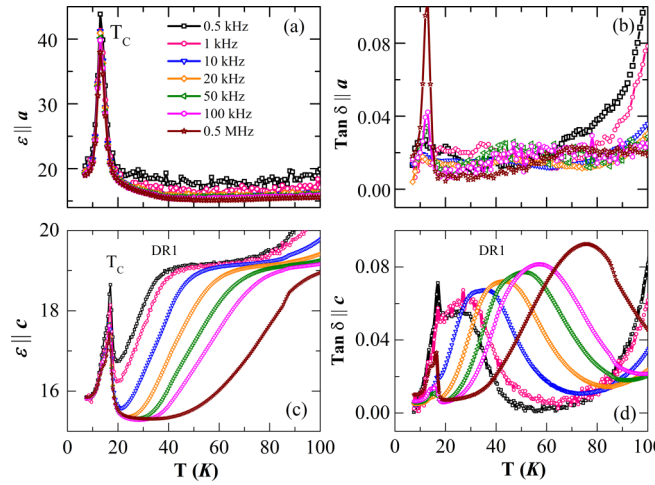

FIG. 4. Dielectric and loss data measured under various frequencies along a axis (a), (b) and c axis (c), (d).

consistent with the peak in the loss behavior seen in Figs. 4(c) and 4(d). The frequency-dependent thermal shift in the steps of ε' and peaks in the loss corresponds to a typical relaxation behavior which was already observed in other multiferroic rare-earth manganites and attributed to Debye-like relaxation due to the presence of localized charge carriers (LCC) in the crystal [23–25]. Fitting the relaxation time constant with inverse temperature to both Arrhenius and Mott insulator related variable range-hopping (VRH) conduction mechanism, we found that it follows the VRH conduction mechanism [see Supplemental Material, Fig. S2(a)] [22]. Further, we notice a straight-line-like behavior with large slope in the complex impedance plot at 45 K [see Supplemental Material, Fig. S2(b)] [22] which suggests the intrinsic nature of the relaxation. Importantly, we notice that this relaxation extends to a wide range of temperature including ferroelectric, paraelectric, and paramagnetic where we see the memory effect. Usually these LCC can be made up of trapped electrons accompanied by lattice distortion [26]. The electron hopping, associated with lattice distortion, behaves like dipole reorientation under ac electric field and can show the dipolar relaxation behavior as observed in the present case. The anisotropic behavior of dielectric relaxation data can be explained by the Jahn-Teller distortion associated with Mn^{3+} ions which is responsible for the relaxation [24]. Since the relaxation has an anisotropic feature, we attempted to find out its correlation to the magnetic ordering. We did not see any distinct anomaly in M vs T for $H||c$ corresponding to the Mn^{3+} spin ordering at $T_N = 39.5$ K; however, the anisotropy can be noticed in the magnetization along the different axis above T_N (see Supplemental Material, Fig. S3) [22]. These results suggest a short-range magnetic correlation above T_N which is in agreement with an earlier report where a nonzero contribution of the magnetic specific heat up to 200 K in the known multiferroic manganite $TbMnO_3$ ($T_N = 41$ K) has been shown [27]. In addition, a nonzero contribution of dielectric constant, related to electromagnon, was observed above T_N in the mixed rare-earth manganite [11]. Very recently, Elsässer *et al.* found a local cycloidal spin order, i.e., electromagnons in $RMnO_3$ compounds persisting up to twice the global

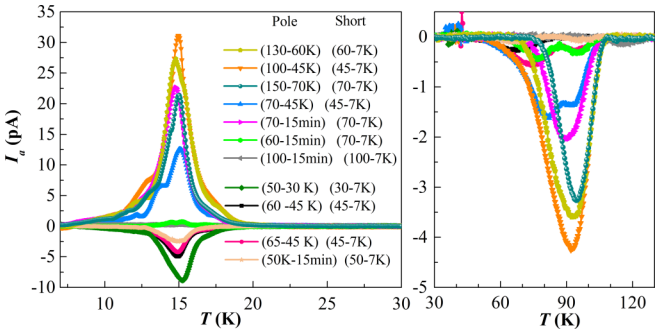

FIG. 5. Pyrocurrent data recorded after poling the sample for different temperature intervals with poling field 5.6 kV/cm.

antiferromagnetic ordering temperature of Mn^{3+} spins [28]. All these studies suggest that the localized charge carriers are strongly correlated to the local short-range magnetic domains at higher temperatures. Thus, it is likely that an internal electric field ($E_{\text{int}}^{\text{LCC}}$) can be produced corresponding to the defect dipoles with the application of external electric field E_{ext}.

Similar to other manganites, a large relaxation behavior above 90 K was observed in the dielectric constant along both $c-$ and a axes (not shown) which can be attributed to the Maxwell-Wagner-type relaxation due to formation of surface barrier layer capacitor at the sample and electrode interface [29]. The charges accumulated at the interface (also called thermally stimulated free charge carriers) under applied electric field can be frozen below the activation temperature and can act as an internal electric field ($E_{\text{int}}^{\text{TSFC}}$) below the freezing temperature (T_f). The consequences of this TSFC carrier-related field at the electrode interface or grain boundary with ferroelectric polarization are well known in the multiferroic materials [30,31]. Here, we observed a TSFC carrier-related pyrocurrent peak at 90 K when the sample was poled from 150 to 40 K and measured from 40 to 150 K which confirms the presence of $E_{\text{int}}^{\text{TSFC}}$ below $T_f \sim 70$ K (TSFC-related pyropeak onset) (see Supplemental Material, Fig. S4) [22]).

C. Origin of memory effect

In order to find the correlation of both $E_{\text{int}}^{\text{LCC}}$ and $E_{\text{int}}^{\text{TSFC}}$ to the memory effect, we recorded the pyrocurrent with different poling temperature interval systematically across the two-relaxation temperatures. First, we applied E_{ext} (5.6 kV/cm) to the sample from 130 to 60 K and subsequently cooled the sample to 7 K with $E_{\text{ext}} = 0$, then measured the pyrocurrent from 7 to 130 K. A positive pyrocurrent peak at T_C and a negative pyrocurrent peak at 90 K are observed. This is in contrast to the pyrocurrent peak at T_C where the sample was poled across T_C as shown in the previous measurements. Since we know that the direction of the $E_{\text{int}}^{\text{TSFC}}$ is opposite to that of the external field as demonstrated earlier [30], we confirm that such pyrocurrent behavior is related to $E_{\text{int}}^{\text{TSFC}}$. A similar pyrocurrent feature is also observed when the sample is poled above 70 K, for example, poling from 100 to 45 K, 150 to 70 K and 70 to 45 K (Fig. 5). However, the external field (E_{ext}) applied at a particular temperature above 70 K produces small peaks or no peak in the pyrocurrent, e.g., poling at 100 K for 15 min (gray, left triangle curve in Fig. 3) because of itinerant behavior of TSFC carriers. Further, the TSFC charge carriers are immobile at low temperature ($T < T_f$), so the formation of $E_{\text{int}}^{\text{TSFC}}$ should be negligible when an E_{ext} is applied to the sample at low temperatures. Therefore, we understand that $E_{\text{int}}^{\text{TSFC}}$ is unlikely to cause memory effect as the temperature range of memory effect is observed below the dynamics of TSFC carriers.

Next, we applied the electric field in the range of 60 to 30 K and cooled to 7 K without any external field and measured the pyrocurrent from 7 to 130 K. Intriguingly, we observed a negative pyrocurrent peak at T_C which is in the same direction of E_{ext} field across the T_C but opposite to the $E_{\text{int}}^{\text{TSFC}}$ (Fig. 5). In this poling case, we do not expect any pyrocurrent peak at T_C as the field was applied above T_C or T_N and below T_f. Thus, we argue that an internal electric field ($E_{\text{int}}^{\text{LCC}}$) is produced below T_f owing to the localized charge carriers. This internal field in fact can polarize the ferroelectric dipoles across T_C. It should be noted that $E_{\text{int}}^{\text{LCC}}$ may disappear when the samples becomes conducting at higher temperature. Since the TSFC carriers become mobile above 70 K, the localized charge-carrier dipoles can also vanish and $E_{\text{int}}^{\text{LCC}}$ may disappear above this temperature.

Now, we recall the thermal behavior of P^{TR} [Fig. 3(c)], where we see a steplike increase above 35 K and gradual decrease above 60 K. This behavior resembles the activity of $E_{\text{int}}^{\text{LCC}}$ with temperature and confirms that $E_{\text{int}}^{\text{LCC}}$ is responsible for the memory effect. We note that the ferroelectric poling effect above T_C also resembles the role of defects in ferroelectric materials [32–36]. Such defects can be formed due to oxygen vacancies, compositional defects, or localized lattice distortion. When the defects are charged with external electric field they become defect dipoles (DD)and can act as an intrinsic local internal bias field inside the crystal. This causes occasionally domain pinning (double hysteresis), shifting of P-E hysteresis loop in the ferroelectric materials through internal biasing field [36]. The ferroelectric dipoles align in the same direction of DD since the defects are present in the ferroelectric domain itself and can induce a preference to align the spontaneous ferroelectric domains in the same direction [36]. Therefore, it can align the ferroelectric dipoles locally along the same direction as the external electric field. Since we see that the localized charge carriers are correlated to the short-range spin (Mn^{3+}) ordering in the sample, it is likely that there are tiny polar regions corresponding to small chiral magnetic domains even in the paramagnetic state. Thus, we propose the following model for the observed memory effect.

A schematic diagram consisting of ferroelectric dipole, LCC dipole, and sample/electrode interface dipole, is shown in Fig. 6 to understand memory effect. It shows the stray charges at the electrode and sample interface, causing the internal electric field ($E_{\text{int}}^{\text{TSFC}}$) and has the direction opposite to the external electric field. The red color arrow represents the ferroelectric dipoles. The white arrow represents the local dipoles ordered in parallel to the ferroelectric dipoles. When the external electric field is applied above 30 K, it can polarize the local dipoles and while cooling the sample, despite removing the external field at 30 K, the local dipolar field can induce the ferroelectric domains to make a single domain state macroscopically below the ferroelectric transition. Similarly,

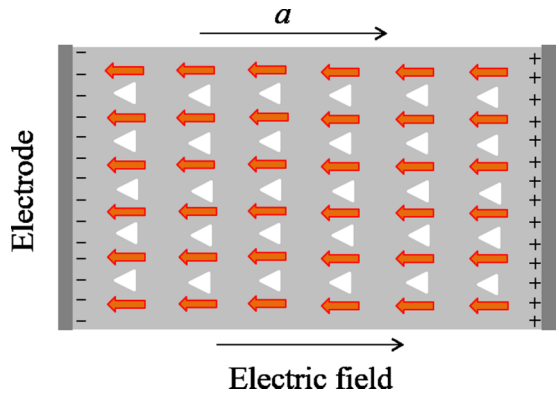

FIG. 6. Schematic diagram of ferroelectric and local dipoles which would orient with the external field once applied and removed. The red arrows and white triangles are corresponding to the ferroelectric and local dipoles, respectively, oriented in the same direction. The charges accumulated on the electrodes are thermally stimulated charge carriers opposite to the external field indicated by the bottom arrow.

when we apply electric field to the sample below 30 K, it poles the macroscopic ferroelectric dipoles and while measuring the pyrocurrent or ramping the temperature above T_C in the absence of field, the local dipoles can be polarized with the depolarization of ferroelectric dipoles and can store the electric potential to carry the microscopic polarization state even above T_N. If the T_R does not exceed ${T_{Mem}}^{Max} \sim T_f$, the stored potential can polarize the ferroelectric dipoles again while cooling the sample through T_C. In this way the LCC dipoles polarize the ferroelectric dipoles in the cooling process, thus a polarization current appears (Fig. 2, dotted curves) and the ferroelectric dipoles restore the field to the LCC in the warming process, hence a depolarization curve appears (Fig. 2, continuous curves). This cyclic process between LCC dipoles and ferroelectric dipoles can continue until the T_R goes above ${T_{Max}}^{Mem}$. Initially, the memory effect decreases as it is expected to occur and the polarization should vanish while crossing the T_C. The dipolar reorientation should increase with the increasing temperature due to thermal energy. In addition, the relaxation dynamics can be slow, which requires sufficient time for the maximum alignment of relaxer dipoles. Thus, with increasing the ramping temperature the local dipoles gets more and more aligned and store the polarization memory. As a result, we see an increasing trend of memory on top of the natural decreasing curve. At much higher temperature the conductivity increases due to the TSFC carrier, which destroys the dipole ordering. Therefore, a decreasing of P_{TR} occurs after ~60 K and completely vanishes at ~80 K which is above the onset of TSFC carrier-related pyropeak. Thus, our study reveals that this memory effect occurs because of the presence of localized charge dipoles which also helps to polarize the ferroelectric domains by applied field above the ferroelectric T_C. Therefore, the localized charge carriers help to protect the ferroelectric state at higher temperature whereas the thermally stimulated charge carriers destroy them. We argue that this memory effect can exist in other multiferroic materials due to unintended consequence of defects or artificially created defects in the materials which is not necessarily correlated with the short-range magnetic ordering and the temperature can be tuned as high as room temperature. Therefore, avoiding the TSFC effect, this LCC can be advantageous towards the technological applications of multiferroics. This study should motivate further work on microscopic picture of ferroelectric domains and defect dipoles in the multiferroics.

In conclusion, we demonstrated that the ferroelectric polarization state could be restored from a deep paramagnetic region without applying any electric or magnetic field. In fact, the ferroelectric domains can also be polarized with the electric field even above the ordering temperature. We have shown that the temperature profile of the magnetoelectric memory effect corresponds to a relaxation behavior of magnetically active localized charge carriers in the lattice, which is composed of defect dipoles of polar nanoregions. Our findings offer a direction of enabling the multiferroics to be operated even at higher temperatures.

ACKNOWLEDGMENTS

Authors C.D. and A.S. acknowledge Sheikh Saqr Laboratory and International Center for Materials Science at Jawaharlal Nehru Centre for Advanced Scientific Research for providing experimental facilities.

[1] M. M. Vopson, Crit. Rev. Solid State Mater. Sci. **40**, 223 (2015).
[2] N. A. Spaldin and M. Fiebig, Science **309**, 391 (2005).
[3] S.-W. Cheong and M. Mostovoy, Nat. Mater. **6**, 13 (2007).
[4] T. Aoyama, K. Yamauchi, A. Iyama, S. Picozzi, K. Shimizu, and T. Kimura, Nat. Commun. **5**, 4927 (2014).
[5] Y. Tokura, S. Seki, and N. Nagaosa, Rep. Prog. Phys. **77**, 076501 (2014).
[6] S. Dong, J.-M. Liu, S.-W. Cheong, and Z. Ren, Adv. Phys. **64**, 519 (2015).
[7] H. Béa, M. Gajek, M. Bibes, and A. Barthélémy, J. Phys.: Condens. Matter **20**, 434221 (2008).
[8] A. Pimenov, A. Mukhin, V. Y. Ivanov, V. Travkin, A. Balbashov, and A. Loidl, Nat. Phys. **2**, 97 (2006).
[9] I. Kézsmárki, U. Nagel, S. Bordács, R. S. Fishman, J. H. Lee, H. T. Yi, S. W. Cheong, and T. Rõõm, Phys. Rev. Lett. **115**, 127203 (2015).
[10] S. Toyoda, N. Abe, S. Kimura, Y. H. Matsuda, T. Nomura, A. Ikeda, S. Takeyama, and T. Arima, Phys. Rev. Lett. **115**, 267207 (2015).
[11] A. Pimenov, A. Loidl, A. A. Mukhin, V. D. Travkin, V. Yu. Ivanov, and A. M. Balbashov, Phys. Rev. B **77**, 014438 (2008).
[12] K. Taniguchi, N. Abe, S. Ohtani, and T. Arima, Phys. Rev. Lett. **102**, 147201 (2009).
[13] I. Fina, V. Skumryev, D. O'Flynn, G. Balakrishnan, and J. Fontcuberta, Phys. Rev. B **88**, 100403(R) (2013).
[14] I. Fina, L. Fàbrega, X. Martí, F. Sánchez, and J. Fontcuberta, Phys. Rev. Lett. **107**, 257601 (2011).
[15] M. Schiebl, A. Shuvaev, A. Pimenov, G. E. Johnstone, V. Dziom, A. A. Mukhin, V. Yu. Ivanov, and A. Pimenov, Phys. Rev. B **91**, 224205 (2015).
[16] M. Mochizuki and N. Furukawa, Phys. Rev. B **80**, 134416 (2009).

[17] A. Pimenov, A. Shuvaev, A. Mukhin, and A. Loidl, J. Phys.: Condens. Matter **20**, 434209 (2008).
[18] S. B. Wilkins, T. R. Forrest, T. A. W. Beale, S. R. Bland, H. C. Walker, D. Mannix, F. Yakhou, D. Prabhakaran, A. T. Boothroyd, J. P. Hill, P. D. Hatton, and D. F. McMorrow, Phys. Rev. Lett. **103**, 207602 (2009).
[19] T. Finger, D. Senff, K. Schmalzl, W. Schmidt, L. P. Regnault, P. Becker, L. Bohatỳ, and M. Braden, Phys. Rev. B **81**, 054430 (2010).
[20] C. De and A. Sundaresan, App. Phys. Lett. **107**, 052902 (2015).
[21] C. De, R. Bag, S. Singh, F. Orlandi, P. Manuel, S. Langridge, M. K. Sanyal, C. N. R. Rao, M. Mostovoy, and A. Sundaresan, Phys. Rev. Mater. **3**, 044401 (2019).
[22] See Supplemental Material at http://link.aps.org/supplemental/10.1103/PhysRevB.100.104407 containing the details of pyroelectric, dielectric, magnetization, and polarization data.
[23] T. Goto, T. Kimura, G. Lawes, A. P. Ramirez, and Y. Tokura, Phys. Rev. Lett. **92**, 257201 (2004).
[24] F. Schrettle, P. Lunkenheimer, J. Hemberger, V. Yu. Ivanov, A. A. Mukhin, A. M. Balbashov, and A. Loidl, Phys. Rev. Lett. **102**, 207208 (2009).
[25] J. Yang, J. He, J. Zhu, W. Bai, L. Sun, X. Meng, X. Tang, C.-G. Duan, D. Remiens, and J. Qiu, Appl. Phys. Lett. **101**, 222904 (2012).
[26] S. Liu and R. Cohen, Appl. Phys. Lett. **111**, 082903 (2017).
[27] D. O'Flynn, M. R. Lees, and G. Balakrishnan, J. Phys.: Condens. Matter **26**, 256002 (2014).
[28] S. Elsässer, M. Schiebl, A. Mukhin, A. Balbashov, A. Pimenov, and J. Geurts, New J. Phys. **19**, 013005 (2017).
[29] P. Lunkenheimer, S. Krohns, S. Riegg, S. G. Ebbinghaus, A. Reller, and A. Loidl, Eur. Phys. J. Spec. Top. **180**, 61 (2009).
[30] C. De, S. Ghara, and A. Sundaresan, Solid State Commun. **205**, 61 (2015).
[31] T. Ngo, U. Adem, and T. Palstra, Appl. Phys. Lett. **106**, 152904 (2015).
[32] P. Gao, C. T. Nelson, J. R. Jokisaari, S.-H. Baek, C. W. Bark, Y. Zhang, E. Wang, D. G. Schlom, C.-B. Eom, and X. Pan, Nat. Commun. **2**, 591 (2011).
[33] Y. Pu, J. Zhu, X. Zhu, Y. Luo, M. Wang, X. Li, J. Liu, J. Zhu, and D. Xiao, J. Appl. Phys. **109**, 044102 (2011).
[34] S. M. Yang, S. J. Moon, T. H. Kim, and Y. S. Kim, Curr. Appl. Phys. **14**, 757 (2014).
[35] C. Folkman, S. Baek, C. Nelson, H. Jang, T. Tybell, X. Pan, and C. Eom, Appl. Phys. Lett. **96**, 052903 (2010).
[36] D. Lee, H.-S. Kim, S. Y. Jang, K. W. Joh, T. W. Noh, J. Yu, C. E. Lee, and J.-G. Yoon, Phys. Rev. B **81**, 012101 (2010).